JCTC Journal of Chemical Theory and Computation

QM-MM Investigation of the Reaction of Peroxynitrite with Carbon Dioxide in Water

Mariano C. González Lebrero and Darío A. Estrin*

Departamento de Química Inorgánica, Analítica y Química Física − INQUIMAE-CONICET, Facultad de Ciencias Exactas y Naturales, Universidad de Buenos Aires, Ciudad Universitaria, Pabellón 2, C1428EHA, Buenos Aires, Argentina

Received February 13, 2007

Abstract: We have investigated the reaction of peroxynitrite with carbon dioxide in aqueous solution by means of combined quantum-classical (QM-MM) molecular dynamics simulations. In our QM-MM scheme, the reactant was modeled using density functional theory with a Gaussian basis set, and the solvent was described using the mean-field TIP4P force field. The free energy profile of this reaction has been computed using umbrella sampling and multiple steering molecular dynamics (MSMD) schemes. Umbrella sampling methods turned out to be much more efficient than MSMD schemes, due to the possibility of employing a combination of classical and QM-MM thermalization schemes. We found the presence of a significant barrier in the free energy profile associated with the reaction in solution, which is not present in vacuum, that may be ascribed to the significant charge redistribution upon reaction and the concomitant solvation pattern changes.

1. Introduction

Peroxynitrite anion ($ONOO^-$) is a stable species formed by the reaction of superoxide with nitric oxide in biological environments.[1] The formation of peroxynitrite has been linked to pathology. Research efforts directed to understand the mechanism of reaction of peroxynitrite were initially focused primarily on the reactions of peroxynitrite with substrates with zero-order kinetics (e.g., dimethyl sulfoxide and deoxyribose), with substrates with relatively small second-order rate constants (e.g., methionine and ascorbate), and with a few more reactive substrates, such as thiols.[1−4] Although these experiments afforded important mechanistic information, the reactions of peroxynitrite with these substrates cannot compete with the reaction of peroxynitrite with CO_2 under physiological conditions, due to the relative high concentration of CO_2 in cellular environment and the fast reaction of these two compounds.

The reaction of peroxynitrite with carbonate buffers was observed initially by Keith and Powel,[5] but its physiological importance was not recognized until 1993 when Radi et al. noted the biological relevance of this reaction.[6]

A possible mechanism for this reaction was proposed in 1995.[3] It is now firmly established that the reaction of peroxynitrite with CO_2 occurs between the peroxynitrite anion ($ONOO^-$) and dissolved CO_2 and forms the carbonate radical ($CO_3^{\bullet -}$) and nitrogen dioxide ($NO_2^{\bullet}$), as shown in Scheme 1.

Electronic structure calculations of the first step of this reaction, the formation of the adduct nitrosoperoxycarbonate, at different levels of theory show that the reaction is barrierless in vacuum.[7] On the other hand, the experimental results in aqueous solution suggest the presence of a significant free energy barrier (about 12 kcal/mol).[8] This fact indicates that the solvent plays a crucial role in the reaction, making it an ideal benchmark for explicit solvent QM-MM methodologies. In this work we have performed molecular dynamics simulations of the reaction in aqueous solution employing a QM-MM strategy to obtain free energy profiles and to understand the reaction mechanism from an atomistic point of view. We critically evaluate the performance of two different advanced sampling tools in the context of QM-

* Corresponding author phone: 54-11-4576-3368; fax: 54-11-4576-3341; e-mail: dario@qi.fcen.uba.ar.

10.1021/ct700038w CCC: $37.00
Published on Web 06/07/2007

Scheme 1. Reaction Pathways for Peroxynitrite in Vivo

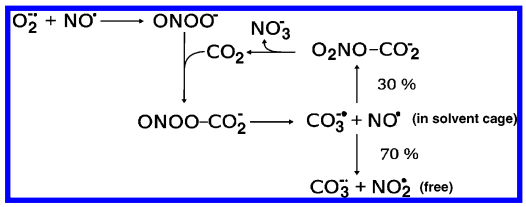

MM calculations, namely, umbrella sampling and multiple steering molecular dynamics schemes.

2. Model and Simulation Methods

The Hybrid QM/MM Hamiltonian. Our computational scheme was constructed by partitioning the system into a quantum-mechanical (QM) and a classical-mechanical (MM) subsystems. Considering a configuration of N_c atoms in the MM subsystem with coordinates and partial charges $\{R_l, q_l, l = 1,...,N_c\}$ and N_q atoms in the QM subsystem with coordinates and nuclear charges $\{\tau_a, z_a, a = 1,...,N_q\}$, we propose the following expression for the ground state, Born−Oppenheimer potential energy surface that drives the dynamics of the nuclei

$$E[\{R_i\},\{\tau_\alpha\}] = E_{KS} + E_{QM-MM} + E_{MM} \tag{1}$$

where the first term is a purely QM piece given by the standard Kohn−Sham expression.[9] The second term in eq 1 accounts for the coupling of the QM and MM subsystems and is given by

$$E_{QM-MM} = \sum_{l=1}^{N_C} q_l \int \frac{\rho(r)}{|r - R_l|}\,dr + \sum_{l=1}^{N_C}\sum_{\alpha=1}^{N_q}\left[v_{LJ}(|R_l - \tau_\alpha|) + \frac{q_l z_\alpha}{|R_l - \tau_\alpha|}\right] \tag{2}$$

where v_{LJ} is the Lennard-Jones potential between the classical and quantum part of the system and $\rho(r)$ is the electron density of the QM subsystem. The last term in eq 1 represents the potential energy contribution from the classical solvent potential, treated with the TIP4P mean-field potential.[10]

For the QM region, computations were performed at the generalized gradient approximation (GGA) level, using the BP86[11−13] combination of exchange and correlation functionals. Gaussian basis sets of double-ζ plus polarization quality were employed for the expansion of the one-electron orbitals.[14] The electronic density was also expanded in an auxiliary basis set;[14] the coefficients for the fit were computed by minimizing the error in the Coulomb repulsion energy. The use of this procedure results in an important speedup of the computation.

In order to describe accurately dissociation processes, we have incorporated into our previously developed QM-MM code,[15] a suitable cutoff scheme in the coupling QM-MM of the cutoff radii in the QM-MM component of the energy.[16]

The electron density of the quantum system is given by

$$\rho(r) = \sum_{i=1}^{N_{OCC}} |\psi_i|^2 \tag{3}$$

where each KS molecular orbital, ψ_i, is defined as

$$\psi_i = \sum_k c_i^k g_k(r) \tag{4}$$

where $g_k(r)$ are the contracted basis functions, given by

$$g_k(r) = \sum_{j=1} c_k^j f_j(r) \tag{5}$$

where each $f_j(r)$ is a Gaussian function. Then, the density can be written as

$$\rho = \sum_{i=1}^{N_{OCC}} |\sum_{k,j} c_i^{kj} f_j(r)|^2 \tag{6}$$

The product of two Gaussian functions of exponents α and β, centered on nuclei A and B, respectively, is proportional to another Gaussian function, centered on a point P

$$f_a(\alpha, r - R_A)\, f_b(\beta, r - R_B) = K_{AB}\, f_c(p, r - R_p) \tag{7}$$

where the constant K_{AB} is given by

$$K_{AB} = \left(\frac{2\alpha\beta}{(\alpha+\beta)\pi}\right)\frac{3}{4}\exp\left[-\frac{\alpha\beta}{(\alpha+\beta)|R_A - R_B|^2}\right] \tag{8}$$

The exponent of the new Gaussian function centered in R_p is

$$p = \alpha + \beta$$

and the third center P lies on a line joining the centers A and B

$$R_p = \frac{\alpha R_A + \beta R_B}{\alpha + \beta}$$

Substituting eqs 5−7 into 2, we can express the first term of eq 9 as

$$\sum_{i=1}^{N_C} q_i \int \frac{\rho(r)}{|r - R_i|}\,dr = \sum_j \sum_{i=1}^{N_C} q_i \int \frac{K_j\ f_j(p_j, r - R_{pj})}{|r - R_i|}\,dr \tag{9}$$

A possible way to compute eq 9 when using periodic boundary conditions is to include only the classical point charges located at a distance smaller than R_{cut} from the geometric center (or mass center) of the quantum subsystem, with R_{cut} equal to half the solvent box length.

However, this turns out to yield very poor results in processes in which the spatial extension of the quantum subsystem changes significantly upon reaction. This effect results in a very pronounced shift in the free energy profile when the size of the QM subsystem becomes similar to the box length. This fact has been noted by York et al.[17] in a recent work.

An alternative scheme which alleviates this flaw consists of using a cutoff scheme in which we keep the integrals for

which the classical partial charge is located at a distance smaller than R_{cut} from the R_p corresponding to that integral

$$\sum_{i=1}^{N_C} q_i \int \frac{\rho(r)}{|r - R_i|} dr \cong \sum_{j} \sum_{i=1}^{N_C} q_i \int \frac{K_j \; f_j(p_j, r - R_{p_j})}{|r - R_i|} dr \; |R_i - R_{P_j}| < R_{cut} \quad (10)$$

Molecular Dynamics Simulations. In all our simulation experiments, the coordinate Verlet algorithm[18] was employed to integrate Newton's equations of motion with a time step of 0.2 fs. Constraints associated with the intramolecular distances in water were treated using the SHAKE algorithm.[19] The Lennard-Jones parameters for the quantum subsystem atoms are ϵ and σ of 0.200, 0.155, and 1.70 kcal/mol and 3.900, 3.154, and 3.65 Å, for N, O, and C, respectively. The solute was solvated in a cubic box of size $a = 24$ Å, containing 497 water molecules. Initial configurations were generated from preliminary 100 ps classical equilibration runs in which the quantum solute was replaced by a rigid peroxynitrite (or adduct) with partial charges obtained from a Mulliken population analysis in vacuo. At $t = 0$, the classical solute is replaced by a solute described at the DFT level, according to the hybrid methodology described above. An additional 2 ps of equilibration was performed using the QM−MM scheme. During the simulations, the temperature was held constant at 298 K by the Berendsen thermostat.[20] The solute and the rest of the system were coupled separately to the temperature bath. In order to compare solvation structures additional equilibrium simulations were performed for the reactants and products in water boxes with 497 solvent molecules and 24 Å of side.

If the free energy barriers are of the same order of magnitude as the thermal fluctuations, it is feasible to obtain the free energy profiles associated with a given process directly from the MD simulations. However, to have an appropriate sampling in accessible simulation times, the barriers should be smaller than thermal fluctuations. In cases where barriers are suspected to be high, biased sampling is required to obtain the free energy profile, also called potential of mean force (PMF). We will present here two different biased sampling methods: umbrella sampling and steered molecular dynamics.

Umbrella Sampling. This method[21] attempts to overcome the sampling problem by modifying the potential function so that the unfavorable states are sampled sufficiently. The potential function is modified by adding a weighting function that usually takes a harmonic form. An umbrella sampling calculation involves a series of stages (called simulation windows), each characterized by a particular value of the reaction coordinate. The PMF is then obtained by superposing the results obtained for all the series of windows.

Multiple Steering Molecular Dynamics. The multiple steering molecular dynamics (MSMD) approach, originally proposed by Jarzynski,[22] is based on the following relation

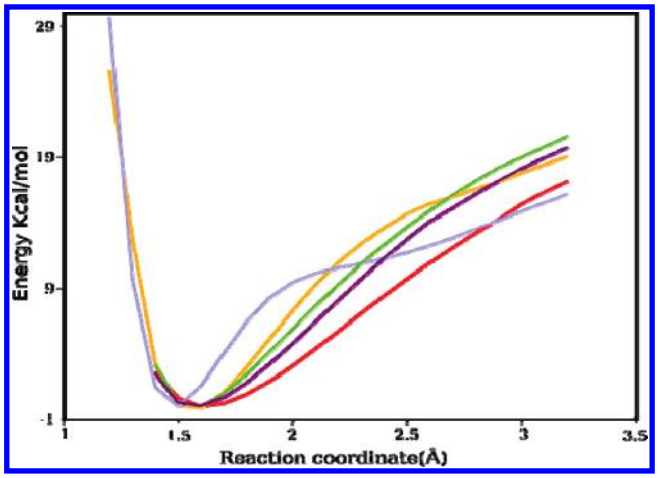

Figure 1. Potential energy profiles for the $ONOO^- + CO_2 \rightarrow ONOOCO_2^-$ reaction. Results obtained using MP2, HF, B3LYP, BP86, and BLYP are depicted in orange, blue, green, violet, and red lines, respectively.

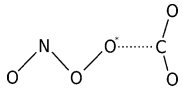

Figure 2. Schematic representation of the reactants. The reaction coordinate is depicted with a dotted line.

between the nonequilibrium dynamics and equilibrium properties

$$\exp[-\Delta A(\xi)\}/k_B T] = \langle \exp[-W(\xi)/k_B T] \rangle \quad (11)$$

in which $W(\xi)$ is the external work performed on the system as it evolves from the initial to the final state along the reaction coordinate ξ.

In MSMD the original potential is modified by adding to the potential energy a time-dependent external potential, usually harmonic, that moves the system along the reaction coordinate by varying the potential well according to

$$E'(r) = E(r) + k[\xi - (\xi_o + v\Delta t)]^2 \quad (12)$$

where v is the pulling speed that moves the system along the reaction coordinate.

The PMF is obtained by performing several MSMD runs, collecting the work done at each time step, and then properly averaging it, according to eq 11. Usually, the pulling speed is chosen so that the system moves smoothly but faster than in a true reversible simulation.[23−25]

Since the averages in this equation are exponential, the results are mostly determined by the trajectories of lower work. This can be addressed by replacing the exponential average by a Taylor expansion and keeping only the terms up to order 2.

For the umbrella sampling method we have taken 9 windows with 100 ps of total integration time. For the steering molecular dynamics method we performed 12 nonequilibrium trajectories going from a reaction coordinate of 1.4−5.4 Å, with a velocity of 0.5 Å/ps and a total time of 96 ps.

Validation of the Method. In order to validate the hybrid Hamiltonian we computed the potential energy profile of the

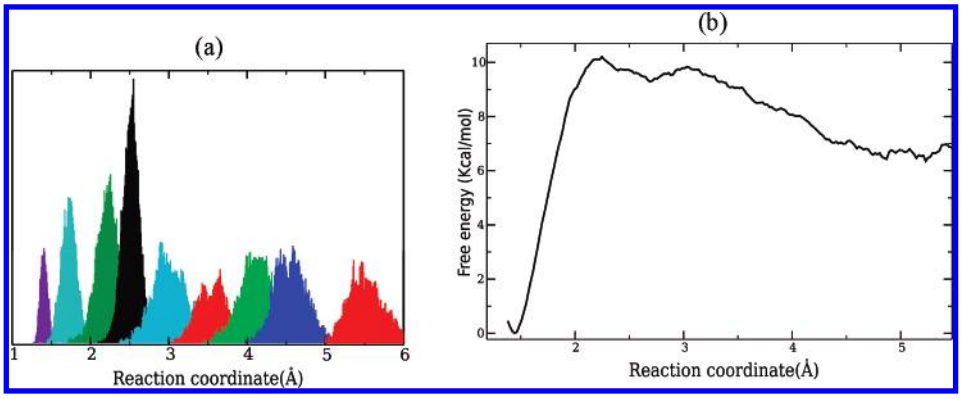

Figure 3. The reaction coordinate histogram for the umbrella sampling simulations (left panel) and the corresponding free energy profile (right panel).

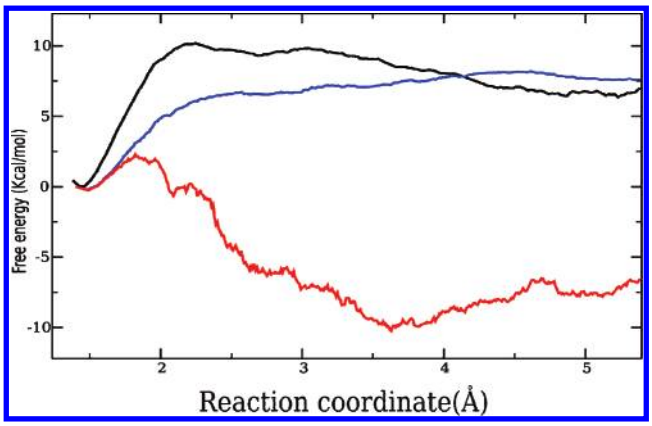

Figure 4. Free energy profile obtained by umbrella sampling (black line), Jarzinski's equation (blue line), and order two truncated expansion of the Jarzinski' s equation (red line).

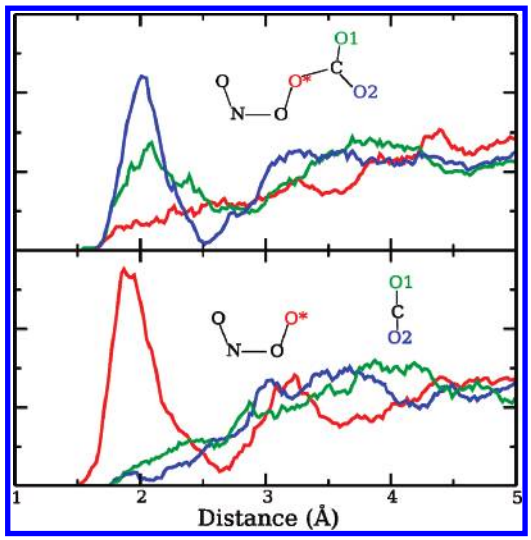

Figure 5. Radial correlation functions of selected atoms with water oxygen atoms from the product (upper panel) and reactant (lower panel). The radial correlations function of the terminal oxygen atom of the peroxynitrite and of the oxygen atoms from the CO_2 are depicted in red, blue, and green, respectively.

reaction in vacuum employing a variety of methods of electronic structure (Hartree Fock, MP2,[26] and DFT using the BP86,[12,13] BLYP,[27] and B3LYP[28] functionals) and the basis set 6-31G**. These calculations have been performed using Gaussian 98[29] (Figure 1).

The reaction coordinate was chosen as the distance between the terminal O of peroxynitrite and the carbon atom from the dioxide, as shown in Figure 2.

It can be seen in Figure 1 that the BP86 functional reproduces correctly the results obtained with more sophisticated methods like MP2 or B3LYP at a significantly lower cost. For this reason we use this functional to describe the QM subsystem.

The Lennard-Jones parameters for the peroxynitrite ion were validated in a previous work,[16] thus only the parameters for the carbon dioxide atoms have to be tested. We have performed an optimization of the adduct ($OONO-CO_2$) with one water molecule attached to one of the oxygen atoms of the CO_2 with the QM-MM and with a full quantum Hamiltonian. The computed binding energies of this aggregate were 12.7 kcal/mol and 11.9 kcal/mol for full quantum and QM-MM calculations, respectively.

3. Results

Umbrella Sampling. The free energy profile was obtained using 9 simulation windows of the umbrella potential, fixed in values that allow a correct sampling of the reaction coordinate range spanning from reactants to products. The total simulation time was 100 ps. The initial structures were thermalized for 100 ps each one with a full classical Hamiltonian, in which the solute was represented for a rigid structure represented with Lennard-Jones and Mulliken charges. Subsequently, 2 ps thermalization have been performed with the hybrid Hamiltonian.

In Figure 3 we show the reaction coordinated histogram for the different windows simulation.

The obtained free energy profile is also shown in Figure 3.

Multiple Steered Molecular Dynamics. The free energy profile was also obtained by using 12 independent steered molecular simulations of 8 ps each one using eq 11. The reaction coordinate was moved from 1.4 to 5.4 Å with a velocity of 0.5 Å /ps. The total simulated time was 96 ps, similar to the total time used in the umbrella sampling calculation. The results obtained using this scheme are shown in Figure 4. The results obtained using umbrella sampling are included for comparison. The significant difference between the results obtained using eq 11 and the results

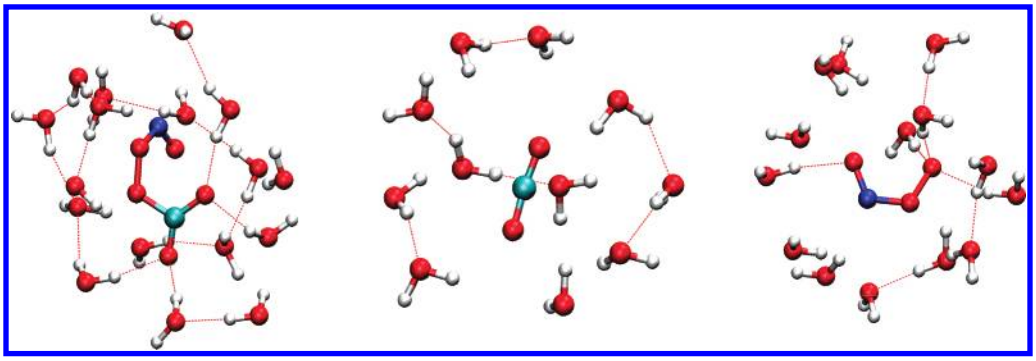

Figure 6. Typical snapshots of the adduct, CO_2, and peroxynitrite (left, middle, and right panels, respectively).

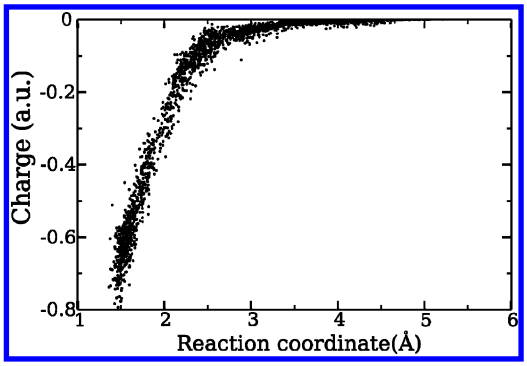

Figure 7. Net Mulliken population on the CO_2 moiety as a function of the reaction coordinate.

obtained using the second-order approximation indicate that there are large statistical errors in using this approach for describing this reaction.

4. Discussion

It can be concluded that the results obtained using the umbrella sampling methodology are more reliable than the results obtained using multiple steered molecular dynamics, for similar total simulation times. This fact can be associated mainly to the steering velocity. Unfortunately, the decrease of this velocity results in an important increase in the already high computational cost. This methodology results inefficiently in systems in which the characteristic relaxation times are not significantly smaller than the accessible total simulation time. In this system the final state of the constrained simulation is far from equilibrium, and this issue generates a systematic error which can only be reduced by decreasing the steering velocity and hence increasing the computational cost. This is due to the fact that there is significant charge redistribution upon reaction, with a concomitant change in solvation patterns which is not represented correctly if the simulation times of the steered molecular dynamics runs are not significantly higher than typical residence times of water molecules. This has also been reported by Cascella in a QM-MM investigation of formamide hydrolysis.[30]

On the other hand, the results obtained using the umbrella sampling with the same total simulation time are more reliable and in qualitative agreement with experimental results. This fact can be related with the extensive thermalization of the different umbrella windows, which improves the convergence of the latter scheme. The hybrid methodology allows us to perform a preliminary (and extensive) thermalization with the full classical Hamiltonian, before switching to the hybrid QM-MM scheme. This combination of classical and QM-MM thermalization schemes improves significantly the efficiency of the umbrella sampling technique compared to multiple steering molecular dynamics techniques at essentially the same computational cost.

The Free Energy Barrier. The free energy profile obtained by the umbrella sampling in aqueous solution shows the existence of a free energy barrier absent in vacuum. This barrier is about 3.8 kcal/mol, which is significantly lower than the experimental estimation. This difference can be tracked down to the DFT electronic structure at the GGA level flaws which typically underestimate the barriers or the absence of polarization effects in the TIP4P force field that can produce also an underestimation of the ion−solvent interaction energies. However, the result is qualitatively correct, and the microscopic view obtained with our simulations can offer important information about the origin of this barrier. In order to get an estimation of the possible DFT flaws in predicting the barriers, we have performed single point calculations of 10 selected snapshots extracted from the simulations, corresponding to reaction coordinates of 2.25 and 1.75 Å (approximate transition state and product, respectively). This provides us an estimation of the activation energy of the reverse reaction. For each snapshot, we have calculated the energy by employing the Gamess-US program[31] at the DFT and MP2 levels, treating the reactant species quantum mechanically, and the 497 water molecules in the simulation box as TIP4P point charges. The average energy difference between the product and the approximate transition state at the MP2 level is 8.6 kcal higher than that calculated using DFT. This indicates that there is indeed an underestimation of the energy barriers by DFT in this case, compared to the MP2 calculations. This DFT flaw is not so evident in the vacuum calculations. The influence of the selected water model has been assessed by means of a scheme in which polarization is modeled by induced point dipoles on the O and H atoms of water molecules due to the electric field of the quantum subsystem as well as other water molecules. These induced dipoles are iterated to self-consistency.[32] We have employed the 10 selected snapshots extracted from the simulations, corresponding to reaction coordinates of 2.25 and 1.75 Å (approximate transition state and product, respectively), and performed single point calculations using TIP4P charges and TIP4P charges plus

induced point dipoles centered at the O and H atoms (1.4146 and 0.0836 Å^3, respectively). The average energy difference between the product and the approximate transition state for the MP2-TIP4P plus polarization is only 2.0 kcal/mol higher than the value computed using the MP2-TIP4P scheme. This indicates that the neglect of solvent polarization results also in the underestimation of the barrier. However, it seems that the errors are smaller than those due to DFT.

In order to obtain an atomistic picture of the solvent effects which produce this barrier, it may be a useful result to analyze the radial distribution function of solute atoms with water oxygen atoms corresponding to products and reactants, shown in Figure 5.

The solvation patterns around the oxygen atoms whose effective charge change during the reaction are, as expected, profoundly modified when going from the reactants to the adduct. In the adduct (upper panel) the oxygen atoms of the carbon dioxide are strongly solvated because they bear a significant high negative charge (Mulliken populations of these atoms are in average −0.55 e). On the other hand, the oxygen of peroxynitrite (O*) is in a hydrophobic part of the molecule and exhibits a weak interaction with water (Mulliken population of this atom is on average −0.25 e). This is confirmed by inspecting typical snapshots (Figure 6).

In the lower panel (reactive) the oxygen atoms of CO_2 (mean values of the Mulliken population of the O atoms are −0.26) are poorly solvated (as expected) and the O* is strongly solvated (mean value of the Mulliken populations for this atom is −0.66). This means that during the reaction the strong hydrogen bonds of the O* atom with water molecules present in the reactant should weaken or break concomitantly with the formation of the adduct. This is probably the main microscopic determinant for the observed free energy barrier. Typical snapshots of CO_2, peroxynitrite, and the adduct in aqueous solution are shown in Figure 6.

The dependence of the net Mulliken population over the CO_2 moiety upon reaction is shown in Figure 7. Since the system negative charge is localized mostly in the oxygen (O*) atom of the peroxynitrite in the reactant and in the oxygen atoms of carbon dioxide in the adduct, the net CO_2 Mulliken charge turns out to be a good indicator of the degree of charge redistribution upon reaction.

In Figure 7 we can see the absence of charge transfer for reaction coordinate values larger than 2.6 Å. This means that the bond is practically broken for longer distances and is consistent with the hypothesis that the barrier is produced by the solvent, since the steep rise in the free energy profile is in the range of reaction coordinates 3.2−4.7 Å, in which the degree of charge transfer indicates that the bond has not yet formed.

5. Conclusion

The reaction of peroxynitrite with carbon dioxide exhibits a barrier in the free energy profile produced by the solvent. The change in the solvation patterns upon reaction is the microscopic determinant of this barrier, since this change implicates the breaking of several hydrogen bonds and the formation of new ones. The results of the QM-MM simulation are in qualitative agreement with the available experimental results. The differences may be due to both the treatment of the experimental data and to limitations of the computational scheme. Umbrella sampling methods turned out to be much more efficient than multiple steered molecular dynamics schemes, due to the possibility with the former methodology to employ a combination of classical and QM-MM thermalization schemes in each simulation window, which is not possible in the MSMD scheme.

Acknowledgment. This work was partially supported by the University of Buenos Aires, Agencia Nacional de Promoción Científica y Tecnológica (project PICT 25667), and CONICET (PIP 5218).

References

(1) Beckman, J. S.; Beckman, T. W.; Chen, J.; Marshall, P. A.; Freeman, B. A. *Proc. Natl. Acad. Sci. U.S.A.* **1990**, *87*, 1620−1624.

(2) Pryor, W. A.; Jin, X.; Squadrito, G. L. *Proc. Natl. Acad. Sci. U.S.A.* **1994**, *91*, 11173−11177.

(3) Squadrito, G. L.; Jin, X.; Pryor, W. A. *Arch. Biochem. Biophys*. **1995**, *322*, 53−59.

(4) Radi, R.; Beckman, J. S.; Bush, K. M.; Freeman, B. A. *J. Biol. Chem*. **1991**, *266*, 4244−4250.

(5) Keith, W. G.; Powell, R. E. *J. Chem. Soc*. **1969**, A, 90−90.

(6) Radi, R.; Cosgrove, T. P.; Beckman, J. S.; Freeman, B. A. *Biochem. J*. **1993**, *290*, 51−57.

(7) Houk, K. N.; Condroski, K. R.; Pryor, W. A. *J. Am. Chem. Soc*. **1996**, *118*, 13002−13006.

(8) Squadrito, G. L.; Pryor, W. A. *Chem. Res. Toxicol*. **2002**, *15*, 885−895.

(9) Kohn, W.; Sham, L. J. *Phys. Rev. A* **1965**, *140*, 1133−1138.

(10) Jorgensen, W. L.; Chandrasekhar, J.; Madura, J. D.; Impey, R. W.; Klein, M. L. *J. Chem. Phys*. **1983**, *79*, 926−935.

(11) Vosko, S. H.; Wilk, L.; Nusair, M. *Can. J. Phys*. **1980**, *58*, 1200−1211.

(12) Perdew, J. P. *Phys. Rev. B* **1986**, *33*, 8822−8824; **1986**, *34*, 7406−7406.

(13) Becke, A. D. *Phys. Rev. A* **1988**, *38*, 3098−3100.

(14) Godbout, N.; Salahub, D. R.; Andzelm, J.; Wimmer, E. *Can. J. Chem*. **1992**, *70*, 560−571.

(15) González Lebrero, M. C.; Bikiel, D. E.; Elola, M. D.; Estrin, D. A.; Roitberg, A. E. *J. Chem. Phys*. **2002**, *117*, 2718−2725.

(16) González Lebrero, M. C.; Perissinotti, L. L.; Estrin, D. A. *J. Phys. Chem. A* **2005**, *109*, 9598−9604.

(17) Nam, K.; Gao, J.; York, D. M. *J. Chem. Theory Comput*. **2005**, *1*, 2−13.

(18) Allen, M. P.; Tildesley, D. J. *Computer Simulation of Liquids*; Clarendon: Oxford, 1987.

(19) Ryckaert, J. P.; Ciccotti, G.; Berendsen, H. J. C. *J. Comput. Phys.* **1977**, *23*, 327−331.

(20) Berendsen, H. J. C.; Postma, J. P. M.; van Gunsteren, W. F.; Di Nola, A.; Haak, J. R. *J. Chem. Phys*. **1984**, *81*, 3684−3690.

(21) Torrie, G. M.; Valleau, J. P. *J. Comput. Phys.* **1977**, *23*, 187−99.

(22) Jarzynski, C. *Phys. Rev. Lett.* **1997**, *78*, 2690−93.

(23) Crespo, A.; Marti, M. A.; Estrin, D. A.; Roitberg, A. E. *J. Am. Chem. Soc*. **2005**, *127*, 940−1.

(24) Park, S.; Schulten, K. *J. Chem. Phys.* **2004**, *120*, 5946−61.

(25) Hummer, G.; Szabo, A. *Proc. Natl. Acad. Sci. U.S.A.* **2001**, *98*, 3658−61.

(26) Krishnan, R.; Pople, J. A. *J. Chem. Phys*. **1980**, *72*, 4244−4245.

(27) Lee, C.; Yang, W.; Parr, R. G. *Phys. Rev. B* **1988**, *37*, 785−789.

(28) Becke, A. D. *J. Chem. Phys*. **1993**, *98*, 5648−5652.

(29) Frisch, M. J.; Trucks, G. W.; Schlegel, H. B.; Scuseria, G. E.; Robb, M. A.; Cheeseman, J. R.; Zakrzewski, J. A.; Montgomery, J. A.; Stratmann, R. E.; Burant, J. C.; Dapprich, S.; Millam, J. M.; Daniels, A. D.; Kudin, K. N.; Strain, M. C.; Farkas, O.; Tomasi, J.; Barone, V.; Cossi, M.; Cammi, R.; Mennucci, B.; Pomelli, C.; Adamo, C.; Clifford, S.; Ochterski, J.; Petersson, G. A.; Ayala, P. Y.; Cui, Q.; Morokuma, K.; Malick, D. K.; Rabuck, A. D.; Raghavachari, K.; Foresman, J. B.; Cioslowki, J.; Ortiz, J. V.; Stefanov, B. B.; Liu, G.; Liashenko, A.; Piskorz, P.; Komaromi, I.; Gomperts, R.; Martin, R. L.; Fox, D. J.; Keith, T.; Al-Laham, M. A.; Peng, C. Y.; Nanayakkara, A.; Gonzalez, C.; Challacombe, M.; Gill, P. M. W.; Johnson, B. G.; Chen, W.; Wong, M. W.; Andres, J. L.; Head-Gordon, M.; Replogle, E. S.; Pople, J. A. *Gaussian 98, Revision A.1*; Gaussian, Inc.: Pittsburgh, PA, 1998.

(30) Cascella, M.; Raugei, S.; Carloni, P. *J. Phys. Chem. B* **2004**, *108*, 369−375.

(31) Schmidt, M. W.; Baldridge, K. K.; Boatz, J. A.; Elbert, S. T.; Gordon, M. S.; Jensen, J. H.; Koseki, S.; Matsunaga, N.; Nguyen, K. A.; Su, S. J.; Windus, T. L.; Dupuis, M.; Montgomery, J. A. *J. Comput. Chem*. **1993**, *14*, 1347−1363.

(32) Li, H.; Netzloff, H. M.; Gordon, M. S. *J. Chem. Phys*. **2006** *125*, 194103-

CT700038W